References

BECKER, P. & COPPENS, P. (1974). *Acta Cryst.* A**30**, 129–147.
BELJERS, H. G., BONGERS, P. F., VAN STAPELE, R. P. & ZIJLSTRA, H. (1964). *Phys. Lett.* **12**, 81–82.
BIRD, B. D., COOKE, E. A., DAY, P. & ORCHARD, A. F. (1974). *Philos. Trans. R. Soc. London Ser. A*, **276**, 277–339.
CHANDLER, G. S., FIGGIS, B. N., PHILLIPS, R. A., REYNOLDS, P. A. & WILLIAMS, G. A. (1982). *Proc. R. Soc. London Ser. A*, **384**, 31–48.
CHANDLER, G. S. & PHILLIPS, R. A. (1986). *J. Chem. Soc. Faraday Trans.* 2, **82**, 573–592.
CLEMENTI, E. & ROETTI, C. (1974). *At. Data Nucl. Data Tables*, **14**, 177–478.
COPPENS, P. & HAMILTON, W. C. (1970). *Acta Cryst.* A**26**, 71–83.
COPPENS, P. (1978). In *Neutron Diffraction*, edited by H. DACHS. Berlin: Springer-Verlag.
FIGGIS, B. N., GERLOCH, M. & MASON, R. (1964*a*). *Acta Cryst.* **17**, 506–508.
FIGGIS, B. N., GERLOCH, M. & MASON, R. (1964*b*). *Proc. R. Soc. London Ser. A*, **279**, 210–228.
FIGGIS, B. N., MASON, R., SMITH, A. R. P. & WILLIAMS, G. A. (1980). *Acta Cryst.* A**36**, 509–512.
FIGGIS, B. N. & REYNOLDS, P. A. (1986). *Int. Rev. Phys. Chem.* **5**, 265–272.
FIGGIS, B. N., REYNOLDS, P. A. & WHITE, A. H. (1987). *J. Chem. Soc. Dalton Trans.* pp. 1737–1745.
IBERS, J. & HAMILTON, W. C. (1974). Editors. *International Tables for X ray Crystallography*, Vol. 4. Birmingham: Kynoch Press. (Present distributor Kluwer Academic Publishers, Dordrecht.)
JOHANSEN, H. & ANDERSEN, N. K. (1986). *Mol. Phys.* **58**, 965–975.
KASPER, J. S. & LONSDALE, K. (1967). In *International Tables for X-ray Crystallography*, Vol. 2. Birmingham: Kynoch Press. (Present distributor Kluwer Academic Publishers, Dordrecht.)
LE PAGE, Y. & GABE, L. J. (1979). *Acta Cryst.* A**35**, 73–78.
MESS, K. W., LAGENDIJK, E., CURTIS, D. A. & HUISKAMP, W. (1967). *Physica*, **34**, 126–148.
PELLETIER-ALLARD, N. (1964). *C. R. Acad. Sci.* **258**, 1215–1220.
POWELL, H. M. & WELLS, A. F. (1935). *J. Chem. Soc.* pp. 359–362.
REYNOLDS, P. A., FIGGIS, B. N. & WHITE, A. H. (1981). *Acta Cryst.* B**37**, 508–513.
SHANNON, R. D. (1976). *Acta Cryst.* A**32**, 751–767.
THORNLEY, F. R. & NELMES, R. J. (1974). *Acta Cryst.* A**30**, 748–757.
VAN STAPELE, R. P., BELJERS, H. G., BONGERS, P. F. & ZIJLSTRA, H. (1966). *J. Chem. Phys.* **44**, 3719–3725.
VIDAL-VILAT, G., VIDAL, J. P. & KURKI-SUONIO, K. (1978). *Acta Cryst.* A**34**, 594–602.
WIELINGA, R. F., BLOTE, H. W. J., ROEST, J. A. & HUISKAMP, W. J. (1967). *Physica*, **34**, 223–240.
WILLIAMS, G. A., FIGGIS, B. N. & MOORE, F. H. (1980). *Acta Cryst.* B**36**, 2893–2897.

Acta Cryst. (1989). B**45**, 240–247

Relation of the Electron Density Distribution in the $CoCl_4^{2-}$ Ion to the Spin Density and to Theory

BY BRIAN N. FIGGIS,* EDWARD S. KUCHARSKI AND PHILIP A. REYNOLDS

School of Chemistry, University of Western Australia, Nedlands, Western Australia 6009, *Australia*

(*Received* 7 *May* 1988; *accepted* 18 *January* 1989)

Abstract

Based upon the 115 K X-ray data for Cs_3CoCl_5 several valence-orbital refinements were carried out to elucidate features of chemical interest. They gave a $t_2^{3.9(2)}e^{4.2(2)}4s'^{0.4(3)}$ valence-electron configuration for the Co atom, when averaged to cubic symmetry. There is a substantial and important redistribution of charge within all ions, which can be well represented by a thin spherical shell at a radius of *ca* 1·50 Å from each nucleus, but not by any of a number of other models of diffuse density. Deviation from cubic symmetry for the Co atom is marked. The results are quite similar to those of an earlier study on Cs_2CoCl_4, and show the importance of effects in the Cs···Cl bonds reminiscent of covalency. The relationship between those charge density results and the spin density distribution obtained on the same compound by polarized neutron diffraction shows that an advanced level of theoretical treatment is required to account for both experiments.

1. Introduction

This paper draws on the results of the preceding paper (Figgis, Kucharski & Reynolds, 1989*a*) for the charge distribution in Cs_3CoCl_5, on the equivalent results for Cs_2CoCl_4 (Figgis, Reynolds & White, 1987), and on the experimental spin density distribution for Cs_3CoCl_5 (Chandler, Figgis, Phillips, Reynolds & Williams, 1982) to examine the bonding in the $CoCl_4^{2-}$ ion.

Complementary X-ray and polarized neutron diffraction (PND) studies have been made on $Cs_2K[Cr(CN_6)]$ (Figgis, Forsyth & Reynolds, 1987; Figgis & Reynolds, 1987), $(NH_3)_4Ni(NO_2)_2$ (Figgis, Reynolds & Wright, 1983; Figgis, Reynolds & Mason, 1983) and Co(pc) (Williams, Figgis & Mason, 1981; Figgis, Kucharski & Reynolds, 1989*b*) (pc=phthalocyaninato ion). Those systems, while having more chemical

* To whom correspondence should be addressed.

0108-7681/89/030240-08$03.00

Table 1. *Valence parameters from refinement R3 on* Cs_3CoCl_5 *compared with those for* Cs_2CoCl_4

	Parameter	Cs_3CoCl_5	Cs_2CoCl_4*
Cs(1)	'4*d*'	10·1 (3)	9·6 (3)
	'5*s* + *p*'	7·3 (3)	7·2 (4)
	p_{shell}	1·3 (1)	1·6 (2)
	r_{shell} (Å)	1·39 (6)	1·45 (7)
	Total charge	+0·3 (2)	+0·6 (2)
Cs(2)	'4*d*'	9·6 (3)	9·9 (2)
	'5*s*+*p*'	7·6 (2)	7·0 (6)
	p_{shell}	1·6 (2)	0·6 (2)
	r_{shell} (Å)	1·27 (4)	1·60 (1)
	Total charge	+0·2 (2)	+1·6 (2)
Co(1)	$3d-t_2$	3·9 (2)	3·3 (3)
	$3d-e$	4·2 (2)	4·0 (3)
	'4*s*+*p*'	0·4 (3)	1·2 (3)
	p_{shell}	−0·3 (2)	−0·2 (3)
	r_{3d}	1·11 (2)	1·05 (3)
	Total charge	+0·9 (2)	+0·7 (2)
Cl(1)	$(sp)_1$	2·07 (14)	
	$(sp)_2$	$=(sp)_1$	
	$3p_\pi$	2·31 (28)	
	p_{shell}	0·7 (2)	
	r_{3sp} (Å)	0·92 (2)	
	Total charge	−0·1 (2)	
Cl(2)	$(sp)_1$	1·94 (7)	1·93 (8)
	$(sp)_2$	1·74 (7)	1·86 (8)
	$3p_\pi$	3·41 (12)	3·40 (15)
	p_{shell}	0·3 (1)	0·5 (1)
	r_{3sp} (Å)	0·96 (1)	0·97 (1)
	Total charge	−0·4 (1)	−0·7 (1)

* Figgis, Reynolds & White (1987).

interest, are more complex and thus more difficult to study from the standpoint of theory. Theoretical calculations to understand the experiments must, at least, take account of the effects of both electron correlation and of neighbouring ions in the crystal lattice.

2. Constrained valence-orbital refinements

The multipole refinements of the Cs_2CoCl_4 data (Figgis, Reynolds & White, 1987) contained many redundant parameters yet were not sufficiently flexible to describe the rather localized nearest neighbour bonding features present in the Fourier maps. A highly constrained fourth-order valence-orbital model was found to account for all but those local features but use few redundant parameters.

We have applied that same constrained valence-orbital model to the Cs_3CoCl_5 data and called it refinement R3. It reduces the number of valence-related parameters from 37 to 22. Each Cs atom has spherical 5*p*- and 4*p*-like populations, and a thin spherical shell of charge, p^{Cs}_{shell}, at a radius r^{Cs}_{shell} from the nucleus. The Co atom is constrained to cubic symmetry, with $3d_e$ and $3d_{t_2}$ and 4*p* functions, a variable 3*d* radius, and a shell population p^{Cl}_{shell} of radius 1·5 Å. The Cl atoms have 3*s*/3*p* hybrid orbitals, (*sp*), directed along the bond to cobalt for Cl(2) and along *c* for Cl(1). The site symmetry population constraint $(sp)_1 = (sp)_2$ applies for Cl(1). In addition each Cl atom has a $3p_\pi$ population and a p^{Cl}_{shell} population at 1·5 Å radius.

Table 2. *Valence parameters from refinement R4 compared with the spin density experimental results for* Cs_3CoCl_5

	Parameter	Charge	Spin*
Cs(1)	'4*d*'	10·8 (2)	
	'5*s*+*p*'	7·0 (3)	
	p_{shell}	1·0 (1)	
	r_{shell} (Å)	1·51 (7)	
	Total charge	+0·3 (2)	
Cs(2)	'4*d*'	10·4 (2)	
	'5*s*+*p*'	7·0 (2)	
	p_{shell}	1·2 (1)	
	r_{shell} (Å)	1·37 (5)	
	Total charge	+0·4 (1)	
Co(1)	$3d_{xy}$	1·37 (12)	0·86 (2)
	$3d_{xz}$	1·20 (8)	1·00 (2)
	$3d_{yz}$	$=3d_{xz}$	$=3d_{xz}$
	$3d_{z^2}$	1·96 (12)	−0·21 (2)
	$3d_{x^2y^2}$	2·12 (12)	−0·01 (3)
	'$4p_x$'	−0·11 (19)	−0·07 (3)
	'$4p_y$'	$=$'$4p_x$'	$=$'$4p_x$'
	'$4p_z$'	0·65 (27)	0·20 (5)
	Mix (3*d*–4*p*)	−0·56 (120)	1·37 (14)
	r_{3d}	1·077 (8)	0·961 (5)
	Total charge/spin	+0·7 (2)	2·70 (2)
Cl(2)	$(sp)_1$	1·99 (8)	0·024 (9)
	$(sp)_2$	1·84 (7)	0·035 (5)
	$3p_y$	1·70 (7)	0·007 (7)
	$3p_z$	1·87 (7)	0·012 (4)
	r_{3sp}	0·94 (1)	0·99 (4)
	Total charge/spin	−0·4 (2)	0·078 (6)
Cl(1)	$(sp)_1$	2·23 (14)	
	$(sp)_2$	$=(sp)_1$	
	$3p_\pi$	2·72 (28)	
	r_{3sp}	0·91 (1)	
	Total charge/spin	−0·2 (2)	

* Chandler *et al.* (1982).

The positional and thermal parameters were fixed at the values of refinement R1 (previous paper) while the valence model and the nine experimental, scale, multiple-scattering and extinction parameters were varied, employing the data with $|\mathbf{K}| < 0{\cdot}7$ Å^{-1}. The results of the refinement are listed in Table 1. The fit is as good as for the full multipole model (R1′) and much better than for the spherical-atom refinement (R2) of the previous paper. The valence-model results are listed in Table 1, together with those from the Cs_2CoCl_4 experiment for comparison.

In analyzing the PND data on Cs_3CoCl_5 a slightly different constrained valence model was used for the spin density on the $CoCl_4$ fragment (Chandler *et al.*, 1982). The 3*d* and 4*p* parameters on the Co atom were allowed the full non-cubic symmetry of the $\bar{4}2m$ site with a variable 3*d* radius, and a term describing 3*d*–4*p* orbital mixing was introduced with appropriate radial dependence and with the tetrahedral angular dependence of the y_3^{-2} multipole. Each Cl atom had all the symmetry-allowed 3*s*/3*p* hybrid orbitals. The *z* axis of Cl(2) was in the *ab* plane perpendicular to the Cl(2) mirror plane. There were no p_{shell} populations. We used this model on the present Cs_3CoCl_5 data to give refinement R4. The valence-parameter values are given in Table 2 together with those of the spin density analysis. They are very similar to those of refinement

R3. The experimental extinction parameters for refinements R3 and R4 are essentially unchanged from R1.

Figs. 1–3 and 4–6* show respectively residual- and model-density maps based upon refinements R1′ and R4, respectively, calculated in the same three planes as used in the preceding paper for the deformation densities. The residual density is defined in the usual way, as

$$\rho_{res}(\mathbf{r}) = (2/V)\sum_j[F_{obs} - F_{calc}(\text{model R1}')] \times \exp(2\pi i\,|\,\mathbf{K}_j\,|\,.\mathbf{r})$$

and the model density as

$$\rho_{mod}(\mathbf{r}) = (2/V)\sum_j[F_{calc}(\text{model R4}) - F_{calc}(\text{sph. atom})] \times \exp(2\pi i\,|\,\mathbf{K}_j\,|\,.\mathbf{r})$$

where the cell volume is V and the jth reflection has wavevector $\mathbf{K}_j$. F_{obs} is the observed structure factor corrected for anomalous dispersion, with sign assigned from the model. F_{calc}(model R4) is the theoretical structure factor of the model R4, but with no anomalous dispersion. F_{calc}(sph. atom) is obtained from a calculation based upon 'free' Cs^+, Co^{2+} and Cl^- ions with the positional and thermal parameters of R4, again with no anomalous dispersion.

The residual density is the observed density which is not accounted for by model R1′, while the model density shows the valence changes implicit in model R4.

* The model-density maps, Figs. 4–6, have been deposited with the British Library Document Supply Centre as Supplementary Publication No. SUP 51606 (4 pp.). Copies may be obtained through The Executive Secretary, International Union of Crystallography, 5 Abbey Square, Chester CH1 2HU, England.

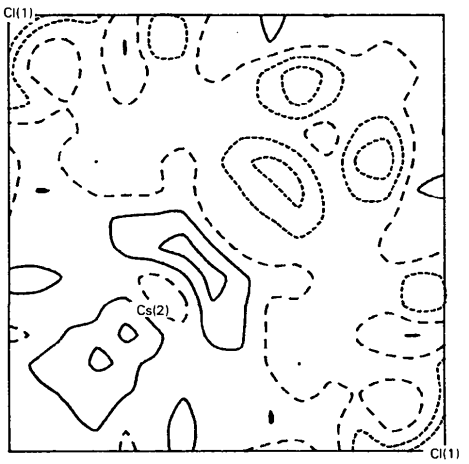

Fig. 1. Residual charge density map for the $z = 0$ plane of Cs_3CoCl_5, containing Cl(1) and Cs(2) based on refinement R1′. The contour interval in this and subsequent maps is 0·2 e Å^{-3}; solid lines for positive, dashed lines for negative density. The plane extends from $x = 0$ to 0·5 and from $y = 0$ to 0·5, downwards, the complete unique area in the plane.

2.1. *Radial changes for the ions*

The above refinements define species that are far from free ions. R5 and R6, listed in Table 3, explore constraints intermediate between refinements R2 (spherical atom) and R4. In refinement R5 we allowed the valence-orbital populations to vary but used their theoretical radial functions. In refinement R6 we allowed both the atom charges and the valence-function radii to vary, but maintained spherical symmetry and included shell populations on the Cs atoms to give further flexibility in the radial-fitting procedure.

A thin shell of charge at radius r_{shell} on each atom may not be the most appropriate model for very diffuse densities. We refined four other aspherical models of density to compare with refinement R4, and details are presented in Table 4. Each such model, except R8, required a uniform density throughout the cell and so affected $F(000)$, whose value was unconstrained.

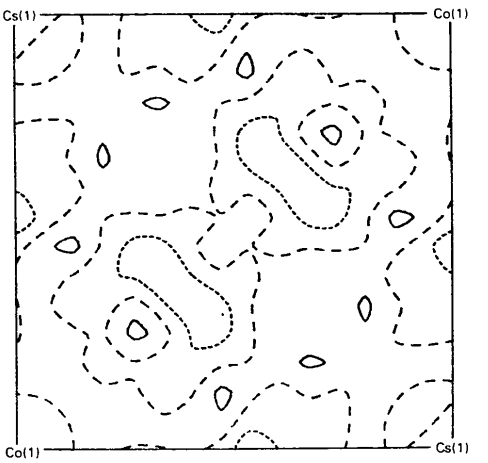

Fig. 2. Residual charge density map for the $z = 0{\cdot}25$ plane of Cs_3CoCl_5, containing Co(1) and Cs(1), with x and y defined as in Fig. 1.

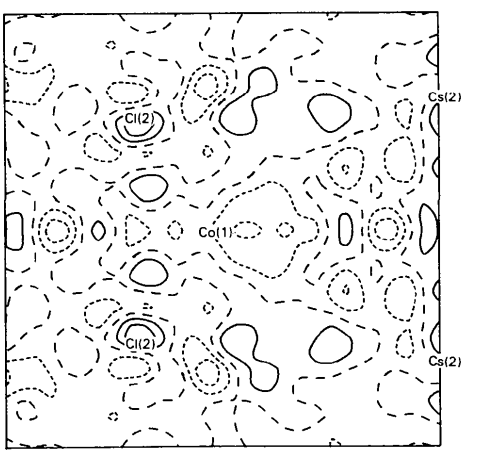

Fig. 3. Residual charge density map for the (110) plane of Cs_3CoCl_5, containing Co(1), Cs(2) and Cl(2).

Table 3. *Ionic charges in* Cs_3CoCl_5

Values without e.s.d.'s in parentheses are assumed and fixed.

		R2	R5	R6 (Aspherical)	R4 (Aspherical)
Cs(1)	Charge	+1·0	+0·9 (2)	+0·2 (2)	+0·3 (2)
	'5s+p'	8·0	8·1 (2)	7·6 (2)	7·0 (3)
	p_{shell}	0·0	0·0	1·1 (1)	1·0 (1)
Cs(2)	Charge	+1·0	+0·9 (1)	+0·4 (2)	+0·4 (1)
	'5s+p'	8·0	8·1 (1)	7·2 (1)	7·0 (2)
	p_{shell}	0·0	0·0	1·4 (1)	1·2 (1)
Co(1)	Charge	+2·0	+2·1 (5)	+0·7 (5)	+0·7 (2)
	3d	7·0	6·8 (1)	7·7 (1)	7·8 (2)
	4p	0·0	0·2 (5)	0·6 (5)	0·4 (3)
	r_{3d}	1·0	1·0	1·08 (1)	1·08 (1)
Cl(2)	Charge	−1·0	−1·0 (1)	−0·4 (2)	−0·4 (2)
	r_{3p}	1·0	1·0	0·94 (1)	0·94 (1)
Cl(1)	Charge	−1·0	−0·6 (1)	−0·2 (1)	−0·2 (2)
	r_{3p}	1·0	1·0	0·90 (2)	0·91 (1)
Agreement factors					
$R(I)$		0·0216	0·0217	0·0149	0·0138
$wR(I)$		0·0233	0·0227	0·0177	0·0159
$R(F)$		0·0100	0·0100	0·0078	0·0071
χ^2		1·010	0·993	0·780	0·709

Refinement R7 corresponds to the model of a uniform density throughout the cell in addition to the normal atomic densities. For refinement R8 density corresponding to a Gaussian function with $\langle U^2 \rangle = 2$ Å^2 and with a refined population was subtracted from each atomic centre, with all populations equal. That is, at each atomic site a scatterer was added with form factor

$$f(\mathbf{K}) = p \exp(-8\pi^2.2\,|\,\mathbf{K}\,|^2),$$

where $\mathbf{K}$ is the wavevector and p the population.

In refinement R9 a uniform sphere of charge with the van der Waals radius was subtracted from each atom site (Cs^+ 1·7, Cl^- 1·8, Co^{2+} 0·75 Å). To compensate, uniform density throughout the cell of opposite sign was added. The models of refinements R8 and R9 differed from that of R7 in that extra density in the interstices between atoms was obtained at the expense of the atom-based contributions.

The scattering factor associated with a uniform sphere of unit density and radius r_m is

$$f_{\text{sphere}} = \int_0^{r_m} 4\pi r^2[\sin(2\pi r\,|\,\mathbf{K}\,|)/(2\pi r\,|\,\mathbf{K}\,|)]\mathrm{d}r$$

$$= [\sin(2\pi r_m\,|\,\mathbf{K}\,|) - (2\pi r_m\,|\,\mathbf{K}\,|) \times \cos(2\pi r_m\,|\,\mathbf{K}\,|)]/2\pi^2\,|\,\mathbf{K}\,|^3.$$

The model of R7 corresponds to the density of −36 (8) e spread uniformly throughout the cell. That of R8 corresponds to 21 (5) e in the Gaussian functions. In the model of R9 −22 (6) e are transferred from within the van der Waals radius to the interstices of the cell, which thus suffer a *depletion* of density. We note that the uniform density does not affect the data directly at all. We estimate it indirectly as follows. We assume the atomic core form factors are correct at the free-ion values. We estimate the valence charge by taking the ratio of valence-to-core charges predicted by the model at $\mathbf{K} = 0$. The difference of the formula charge from the sum of core and valence charges is then the required integrated uniform density.

Table 4. *Results of refinements conducted to examine models of the very diffuse density in* Cs_3CoCl_5

R3 = diffuse density in thin shells; R7 = diffuse density uniformly spread; R8 = diffuse charge in Gaussian atom-centred sites of $\langle U^2 \rangle = 2$ Å^2; R9 = diffuse density uniformly spread, with an equal negative density inside atom-centred volumes of van der Waals radius, *i.e.* uniform density outside van der Waals radii; R10 = diffuse density in thin shells and uniform outside van der Waals radii.

	Population	R3	R7	R8	R9	R10
Cs(1)	Charge	+0·3 (3)	−1·5 (3)	−2·4 (4)	−2·1 (3)	−0·5 (4)
	'5s+p'	−0·7 (3)	1·3 (3)	1·2 (4)	1·7 (2)	0·4 (3)
	p_{shell}	1·3 (1)	0	0	0	0·6 (2)
Cs(2)	Charge	+0·2 (4)	−1·3 (3)	−2·5 (3)	−1·9 (3)	−0·4 (4)
	'5s+p'	−0·4 (2)	1·4 (3)	1·4 (3)	1·7 (2)	0·5 (2)
	p_{shell}	1·6 (2)	0	0	0	0·9 (2)
Co(1)	Charge	+0·9 (3)	+0·5 (3)	+0·2 (3)	+0·1 (4)	+0·6 (3)
	3d	8·1 (3)	7·6 (3)	7·6 (3)	7·7 (3)	8·1 (3)
	4p	0·4 (3)	0·9 (3)	1·1 (4)	1·2 (3)	0·7 (2)
	r_{3d}	1·11 (2)	1·03 (1)	1·03 (1)	1·06 (1)	1·10 (2)
	p_{shell}	−0·3 (2)	0	0	0	−0·3 (2)
Cl(2)	Charge	−0·4 (2)	−1·2 (2)	−1·3 (2)	−0·1 (2)	−0·5 (2)
	r_{3p}	0·96 (1)	0·97 (1)	0·97 (1)	1·06 (2)	1·00 (1)
	p_{shell}	0·7 (2)	0	0	0	0·2 (2)
Cl(1)	Charge	−0·1 (3)	−0·8 (4)	−0·9 (4)	+0·3 (4)	−0·2 (3)
	r_{3p}	0·92 (2)	0·94 (2)	0·94 (2)	1·03 (2)	0·98 (2)
	p_{shell}	0·3 (1)	0	0	0	−0·2 (1)
Uniform density (e cell^{-1})		0	−36 (8)	0	−55 (6)	−30 (5)
Atom-centred density (e) (shell, Gaussian, spheres)		24 (3)	0	+21 (5)	+33 (6)	+18 (4)
Agreement factors						
$R(I)$		0·0136	0·0154	0·0156	0·0150	0·0135
$wR(I)$		0·0158	0·0181	0·0181	0·0181	0·0157
$R(F)$		0·0070	0·0081	0·0081	0·0080	0·0070
χ^2		0·703	0·798	0·801	0·804	0·699

3. Results and discussion

3.1. *Density maps*

The residual maps of Figs. 1–3 from the multipole refinement R1′ show a large reduction in the significant features relative to the deformation maps of the preceding paper, only part of the hole at the Cl(1) position remaining. The model difference density maps, Figs. 4–6 (deposited), resemble the deformation density fairly closely.

3.2. *Ionic deformation in the crystal and the refinements*

By comparing refinements R6 and R4 we see that the major improvement is *not* due to including asphericity in the electron distributions of atoms. By comparing refinements R2 and R5 we see that conventional valence populations have only a relatively small effect. The major improvement is seen in the comparison of

refinements R6 and R5. Allowing the *shape* of the valence form factors to vary has a strong effect. That is just what is predicted on the basis of the direct-summation analysis procedure of the preceding paper. Refinement R6 removes some of the Cs-atom valence-orbital populations and places them in thin shells at refined radii, constituting an approximation to the amount and radius of the changed density. Both changes are about equally effective in improving the goodness of fit. A real system, of course, would have a finite width and defined cross-sectional shape to the shell.

To examine other approximations to the diffuse density at, or outside, the van der Waals radii we compare refinements R4 to R10. From R5 and R6 we see that thin shells of charge can reduce χ^2 by 0·21, an important improvement, but without shells a uniform density raises χ^2 by 0·09, as seen from R4 *versus* R7. Filling the interstices using Gaussian functions (R8) or a uniform density outside the van der Waals radius (R9) each increase χ^2 by *ca* 0·1 from R4. These approximations to the very diffuse density are not as effective as the shells. The models of R7 and R8 put density in the interstices, with the valence functions adjusted accordingly, and give similar results, whereas R4 puts density at the van der Waals radius to give a much better fit. The model of refinement R10 combines shells together with a uniform density outside the van der Waals radius and confirms the picture, giving a marginally better fit than R4. The results of R10 give 6·4 (9) e in the thin shells and −11·4 (23) e in the interstitial region. The 6·4 (9) e in thin shells may be derived by simply summing the shell populations, noting that correlation reduces the apparent error. The interstitial density has a refined value of −0·025 (5) e Å^{-3}. This gives the charge of −30 (6) e over the 1207 Å^3 of the cell, 18 (4) e in the 744 Å^3 van der Waals region and −11 (2) e in the interstitial region. This reduction in density in the interstices, *ca* 0·025 e Å^{-3}, should be viewed in the light of the density at the centre of such a place which could arise from close-packed Cs^+ ions, *ca* 0·050 e Å^{-3}, as pointed out in the preceding paper. Although the thin-shell model is artificial, in fact it is effective and is not improved by any of our simple modifications to make it physically more reasonable.

Examination of Table 1 shows that the ions in the two compounds Cs_2CoCl_4 and Cs_3CoCl_5 (R3) give remarkably similar results. The Cs atoms lose from 0·4 to 1·0 (mean 0·7) electrons from the '$5s + p$' valence region and 0·6 to 1·6 (mean 1·3) electrons appear in the shell at 1·27 to 1·60 (mean 1·42) Å from the nucleus. The '$5s + p$' electrons have a different radial dependence to the shell and they maximize at about half the van der Waals radius. It is well known that the density along an interionic vector such as M–X does not change much between an $M^+\cdots X^-$ and an $M^0\cdots X^0$ formulation of the bonding (Seiler & Dunitz, 1986). However, in the real crystal, our results indicate that the minimum in the density around the centre of the vector is shallower than either the free-ion or the free-atom superpositions predict, and this excess is obtained from nearer to each nucleus. The Cl atoms, whether 'bonded' or 'non-bonded' show a similar phenomenon. In addition, the valence density is contracted from the free-ion theoretical value.

As conventionally depicted, *after hybridization* ('atom preparation'), covalent bonding in diatomic molecules produces little change close to either nucleus, a depletion of charge further along the internuclear vector, and an accumulation of charge in the mid-bond region (Kunze & Hall, 1986; Chandler, unpublished results). This is just what we observe in Cs_3CoCl_5, on a reduced scale. The deformation density closely resembles that of conventional covalent bonding but, of course, the amount of charge shift, 0·1 to 0·15 e per bond, is much less.

The Co atom, in contrast, shows an expansion of the valence functions in real space in both compounds. The 3*d* radii expand by 11(2) and 5(3)%, and quite large '$4s + p$' populations, 0·4(3) and 1·2(3) e, respectively, appear in Cs_2CoCl_4 and Cs_3CoCl_5. This change also suggests a marked electronic interaction of the Co atom with its four Cl(2) neighbours – in other words 'bonding' or covalence. However, the small 'shell' population contrasts with the other ions. Perhaps it reflects the small, relatively unpolarizable nature of transition-metal ions in general and the opportunity to use '$4s/p$' orbitals instead of the 'shell'.

The use of valence functions enables consistent estimates of charges to be made from experiment to experiment although the absolute values are not reliable since a model is required to partition the continuous electron density. We see values for the Cs atom of +0·2 to +1·6 (mean 1·3) units, the Co atom +0·9 to +0·7 in Cs_2CoCl_4 and Cs_3CoCl_5, respectively, the 'bonded' Cl atom −0·4 and −0·7, and the 'non-bonded' Cl atom (in Cs_3CoCl_5) −0·1 units. These values are intermediate between the ideal ionic figure and the zero of the atomic case, as is generally found. The 'non-bonded' Cl atom is far from the ionic value indicating that 'non-bonded' interactions substantially perturb the total charge density. Comparison of the $CoCl_4$ fragment with free-ion $CoCl_4^{2-}$ calculations must be of limited value.

3.3. *Anisotropy in the charge density*

In Cs_3CoCl_5 the Cs atoms appear to have no large anisotropy in the charge density distribution, in contrast to the case of Cs_2CoCl_4. The structure of Cs_3CoCl_5 leads us to expect no anisotropy for Cs(1), but the result for Cs(2) is surprising. The four shortest Cs(2)–Cl distances of the eight are all on one side of the Cs(2) atom, and we might expect an appreciable

value for the (10) dipolar multipole coefficient. In contrast, the polarization of Cl(1) appears to be quadrupolar in symmetry; refinement R1 and the direct analysis both show a large (20) multipole coefficient, and R3 the corresponding low apparent p_π population. This reduction of the valence density in the crystal *ab* plane is just what would be expected from the four short Cs(2)–Cl(1) contacts in that plane, compared with the two longer out-of-plane Cl(1)–Cs(1) contacts.

In the $CoCl_4$ fragment we see that the anisotropy in the Co 3*d* density is appreciable, although that was not apparent in the deformation density maps or direct analysis. The configuration deduced, $t_2^{3.9(2)}e^{4.2(2)}$, is similar to that found for Cs_2CoCl_4, $t_2^{3.3(3)}e^{4.0(3)}$, but differs from the spherical ion $t_2^{4.2}e^{2.8}$ prediction.

Cl(2) has a larger apparent $(sp)_1$ population than for p_π or $(sp)_2$. $(sp)_1$ points at the Co atom, so the result is expected in the absence of covalent transfer of charge. The interionic effects compress the Cl(2) valence density, just as for the other 'non-bonded' ions, while the Co–Cl(2) bond should cause an expansion of $(sp)_1$ just as for the Co 3*d* orbitals. An average (*sp*) or Cl(2) radius, given the correlation of anisotropy in populations and change in radius, could lead to an increase in the observed $(sp)_1$ population, as found in both Cs_2CoCl_4 and Cs_3CoCl_5. Covalent charge transfer from Cl(2) to Co, if any, complicates this picture, as discussed below.

3.4. *Covalence and bonding in the* $CoCl_4^{2-}$ *ion*

3.4.1. Cs_2CoCl_4 *charge density*. In Cs_2CoCl_4 (Figgis, Reynolds & White, 1987) a major feature of the difference density is a large 4(*s*/*p*)-based density on the Co atom along with a small increase in the Co $3d$–t_2 population and decrease in the populations on the Cl atoms. As well as these covalence effects there are substantial interionic influences which affect apparent Cl-atom charges, the apparent ratio of π to σ donation for chlorine, and the radial dependence of the chlorine valence functions, as shown by large shell populations.

3.4.2. Cs_3CoCl_5 *spin density*. The spin density distribution for the $CoCl_4^{2-}$ ion in Cs_3CoCl_5 has been interpreted with a similar bonding explanation to the Cs_2CoCl_4 charge density study (Chandler *et al.*, 1982). The three spins are concentrated mainly in the Co $3d$–t_2 orbitals defined by the crystal field of the tetrahedral anion. Spin appears on the Cl atoms by the donation of charge into the Co $3d$–t_2 orbitals, with σ donation dominating π. The σ/π donation ratio is much better defined and much less affected by interionic effects than for the X-ray experiments. There is a substantial Co 4*p* component in the molecular orbitals since there is mixing in of 4*p* and 3*d* orbitals in the tetrahedral stereochemistry of the anion. The $3d$–e orbitals of the Co atom show evidence of spin polarization in their apparent negative populations.

Comparison with the Cs_2CoCl_4 charge density results showed that the bonding is not described well by simple spin-paired molecular-orbital theory. For example, the decrease in the Co $3d$–t_2 spin population is not nearly as large as the increase in the charge population. Changes in 3*d* radii and 4*s*/*p* populations, amongst other things, point to the importance of spin polarization in the PND data. Spin polarization is a manifestation of electron–electron correlation. Theoretical *ab-initio* calculations should include such correlation but rarely do. The connection between spin and charge densities is complex, so spin and charge density data cannot be interpreted together using single-multipole models with simple relationships between charge and spin populations and with common radii for the valence functions. A fuller discussion of this point would be appropriate only in a more theoretical paper. However, we can note that Deeth, Figgis & Ogden (1988) in their unrestricted $X\alpha$ calculation show for the $CoCl_4^{2-}$ ion, in their Table 1, that spin-up and spin-down orbitals cannot be grouped in pairs with similar covalence parameters. If the covalence and other properties in the up-spin system are not obviously related to those in the down-spin system then it follows that the sum and difference – that is the charge and spin densities – are also unrelated. If that relation is lost in an approximate calculation then further refinement to the 'exact' wave function is unlikely to recover the position.

3.4.3. Cs_3CoCl_5 *charge density*. The present charge density analysis of the Cs_3CoCl_5 data confirms the earlier conclusions. The Co–Cl bonding involves a large Co-atom 4*p* population, increased $3d$–t_2 and unchanged $3d$–e populations, and a decreased Cl-atom population. The '4*p*' population may be slightly less and the $3d$–t_2 population rather more than those for the Cs_2CoCl_4 case. However, using the spin density results on the same compound, we observe that charge transfers are significantly larger than spin transfers, confirming the importance of spin polarization within the anion. The chlorine π/σ donation ratio again appears to suffer from interionic effects. Such ligand polarization by intermolecular influences has been shown more clearly in charge density studies on two compounds containing the $Cr(CN)_6^{3-}$ ion (Figgis, Reynolds & White, 1987; Figgis & Reynolds, 1985).

The Co-atom 3*d* radial expansion, 8(1)%, is significantly larger than for the spin density case, −3·9(5)%. Spin polarization of the filled $3d$–e orbitals tends to reduce the apparent radius of the spin distribution, but the difference may also be a manifestation of a 'differential nephelauxetic effect' in which the 'non-bonded' $3d$–e orbitals have a larger radius than the 'bonded' t_2 orbitals (Craig & Magnusson, 1958).

3.4.4. *Deviations from cubic symmetry*. The observed small distortion from cubic symmetry of the atomic

positions in the $CoCl_4$ fragment has not produced significant changes in calculated deformation and spin densities (Phillips & Chandler, unpublished results). However, both the observed spin and charge densities have significant components of symmetry lower than cubic. The $3d_{xy}$ charge population in Table 2 is higher than that of the $d_{xz,yz}$ pair, but the spin populations are in the reverse order, suggesting that the molecular orbital involving $3d_{xy}$ has a smaller coefficient than those involving $3d_{xz,yz}$. The $4p_z$ population is large in both charge and spin studies, but those of $4p_{x,y}$ are negligible. By symmetry only the $4p_z$ orbital can mix with $3d_{xy}$. There seems to be a consistent picture in which the mixing of $3d_{xy}$ with $4p_z$ is much greater than that of $3d_{xz,yz}$ with $4p_{x,y}$.

This can be interpreted using an energy-level scheme derived by a ligand-field component of tetragonal symmetry acting on the cubic symmetry levels, as shown in Fig. 7. The sign of the tetragonal distortion brings $3d_{xy}$ and $4p_z$ closer and moves $3d_{xz,yz}$ and $4p_{x,y}$ further apart in energy. The net effect is, as required, to give larger mixing of $3d_{xy}$ with $4p_z$ than of $3d_{xz,yz}$ with $4p_{x,y}$. This energy-level scheme has also been deduced experimentally directly from optical spectroscopy (Van Stapele, Beljers, Bongers & Zijlstra, 1966). The observed crystal environment is obviously tetragonally distorted from cubic symmetry. However, it is not possible to define the magnitude, or even the sign, of the splitting of the Co-atom energy levels from simple arguments.

4. Conclusions

The charge density experiment on Cs_3CoCl_5 can be consistently interpreted together with the previous study on Cs_2CoCl_4 and the spin density results only if we consider at least three separate factors of comparable size: (1) the covalence of the Co–Cl bond, (2) the deformations caused by the interionic 'crystal' effects, and (3) the effect of electron–electron correlation on the wavefunction for the $CoCl_4$ unit.

The Cs_2CoCl_4 and Cs_3CoCl_5 charge density results agree well at the various ions. The differences between the two salts may possibly be crystal-environment effects. The Co–Cl bond involves mainly σ donation from the Cl atoms, with a π component, into metal $3d$–t_2 and $4p$ orbitals. The t_2 orbitals gain 0·6(2), the e and $4p$ orbitals 0·7(3) e, averaged over the figures for the two compounds. Substantial spin polarization, caused by electron–electron correlation, reduces the corresponding spin transfers, both expected and observed.

There is a substantial tetragonal component seen in both the charge and spin distributions within the $CoCl_4$ fragment, which may be accounted for by a large $3d_{xy}/4p_z$ mixing. The sign of the distortion agrees with spectroscopic results. Theoretical calculations by *ab-initio* methods give much lower covalent transfers for both charge and spin (Figgis, Reynolds & White, 1987), although recent approximate calculations are more encouraging (Deeth *et al.*, 1988).

The 'non-bonded' interionic interactions, mainly between Cs and Cl atoms, cause substantial changes to the radial distributions of the atoms. Caesium-based and chlorine-based density is removed from outer valence regions, *ca* 0·5 to 1·5 Å from the nuclei, and concentrated at around 1·5 Å, near the van der Waals radius, and appears to be related to weak covalent bonding. The large effects observed here, but apparently not in studies of the lighter alkali-metal salts, may well be due to the high electric polarizability and hyperpolarizability of heavy elements (Mahan, 1980*a*,*b*; McEachran, Stauffer & Greita, 1979).

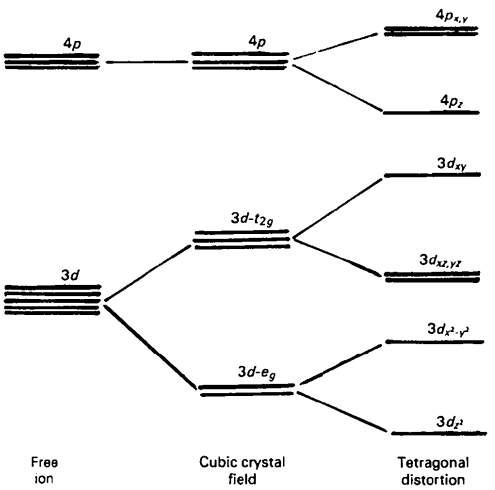

Fig. 7. Schematic diagram for the splitting of the $3d$ and $4p$ orbitals of the Co atom in the $CoCl_4^{2-}$ ion resulting from Co···Cl and Cs···Cl interactions in Cs_3CoCl_5.

The authors are grateful to the Australian Research Grants Scheme for financial support.

References

CHANDLER, G. S., FIGGIS, B. N., PHILLIPS, R. A., REYNOLDS, P. A. & WILLIAMS, G. A. (1982). *Proc. R. Soc. London Ser. A*, **384**, 31–48.

CRAIG, D. P. & MAGNUSSON, E. A. (1958). *Discuss. Faraday Soc.* **26**, 116–122.

DEETH, R. J., FIGGIS, B. N. & OGDEN, M. I. (1988). *Chem. Phys.* **12**, 115–130.

FIGGIS, B. N., FORSYTH, J. B. & REYNOLDS, P. A. (1987). *Inorg. Chem.* **26**, 101–105.

FIGGIS, B. N., KUCHARSKI, E. S. & REYNOLDS, P. A. (1989*a*). *Acta Cryst.* B45, 232–240.

FIGGIS, B. N., KUCHARSKI, E. S. & REYNOLDS, P. A. (1989*b*). *J. Am. Chem. Soc.* In the press.

FIGGIS, B. N. & REYNOLDS, P. A. (1985). *Inorg. Chem.* **24**, 1864–1873.

FIGGIS, B. N. & REYNOLDS, P. A. (1987). *J. Chem. Soc. Dalton Trans.* pp. 1747–1753.
FIGGIS, B. N., REYNOLDS, P. A. & MASON, R. (1983). *J. Am. Chem. Soc.* **105**, 440–443.
FIGGIS, B. N., REYNOLDS, P. A. & WHITE, A. H. (1987). *J. Chem. Soc. Dalton Trans.* pp. 1737–1745.
FIGGIS, B. N., REYNOLDS, P. A. & WRIGHT, S. (1983). *J. Am. Chem. Soc.* **105**, 434–439.
KUNZE, K. L. & HALL, M. B. (1986). *J. Am. Chem. Soc.* **108**, 5122–5127.
MCEACHRAN, R. P., STAUFFER, A. D. & GREITA, S. (1979). *J. Phys. B*, **12**, 3119–3123.
MAHAN, G. D. (1980*a*). *Chem. Phys. Lett.* **76**, 183–185.
MAHAN, G. D. (1980*b*). *Phys. Rev. A*, **22**, 1780–1785.
SEILER, P. & DUNITZ, J. D. (1986). *Helv. Chim. Acta*, **69**, 1107–1112.
VAN STAPELE, R. P., BELJERS, H. G., BONGERS, P. F. & ZIJLSTRA, H. (1966). *J. Chem. Phys.* **44**, 3719–3715.
WILLIAMS, G. A., FIGGIS, B. N. & MASON, R. (1981). *J. Chem. Soc. Dalton Trans.* pp. 734–742.

Acta Cryst. (1989). B**45**, 247–251

Structure Refinements of Lead-Substituted Calcium Hydroxyapatite by X-ray Powder Fitting

BY A. BIGI AND A. RIPAMONTI

Dipartimento di Chimica 'G. Ciamician', Universita' degli Studi, Via Selmi 2, *I*-40126 *Bologna, Italy*

AND S. BRÜCKNER

Dipartimento di Chimica, Politecnico, Piazza Leonardo da Vinci 32, *I*-20133 *Milano, Italy*

AND M. GAZZANO AND N. ROVERI

Centro di Studio per la Fisica delle Macromolecole (CNR), c/o Dipartimento di Chimica, Universita' degli Studi, Via Selmi 2, *I*-40126 *Bologna, Italy*

AND S. A. THOMAS

Department of Chemistry, Ahmadu Bello University, Zaria, Nigeria

(*Received* 22 *August* 1988; *accepted* 6 *February* 1989)

Abstract

The crystal structures of hydroxyapatites, synthesized at different degrees of lead substitution for calcium (20, 45 and 80% Pb atoms) by solid-state reaction at 1173 K, have been investigated by X-ray powder-pattern fitting. The disagreement factors (R_{wp}) are 5·9, 6·0 and 6·6% for Pb20, Pb45 and Pb80, respectively. The site-occupancy factors of Pb atoms indicate a clear preference of lead for site (2) of the apatite structure, which may be responsible for the observed deviations of the *c*-axis dimension from Vegard's law. An increasing shift of the OH group above or below the center of the Pb(2) triangles has been observed with increasing lead content. The JCPDS file Nos. for Pb20, Pb45 and Pb80 are 40-1497, 40-1496 and 40-1495, respectively.

Introduction

The structure of hydroxyapatite (HA) can easily accommodate a great variety of substituents, both anionic and cationic (Lang, 1981; LeGeros & LeGeros, 1984). Among the cations which can be incorporated in the HA structure, only cadmium, strontium and lead are known to replace calcium over the whole range of composition. The *a*- and *c*-axis dimensions of both strontium–calcium apatites and cadmium–calcium apatites vary linearly with composition according to Vegard's law (Heijligers, Driessens & Verbeeck, 1979; Bigi, Gazzano, Ripamonti, Foresti & Roveri, 1986). Lead can substitute for calcium in the HA structure over the whole range of composition causing an enlargement of the unit cell. Although in earlier papers (Muller, 1947; Narasaraju, Singh & Rao, 1972; Rao, 1976) the lattice parameters of lead–calcium hydroxyapatite were reported to vary linearly with the composition, more recently deviations of the *c* parameter from Vegard's law have been observed (Engel, Krieg & Reif, 1975; Verbeeck, Lassuyt, Heijligers, Driessens & Vrolijk, 1981; Andres-Verges, Higes-Rolando, Valenzuela-Calahorro & Gonzalez-Diaz, 1983). The observed deviations from Vegard's law have been attributed to a possible preference of the Pb^{2+} ion for site (2) of the apatite structure, on the basis of the cation distribution deduced from the relative intensities of suitable reflections in the powder diffractogram

0108-7681/89/030247-05$03.00